Atmos. Chem. Phys. Discuss., doi:10.5194/acp-2017-16, 2017
Manuscript under review for journal Atmos. Chem. Phys.
Discussion started: 16 February 2017


Atmospheric Chemistry and Physics Discussions

# Insight into winter haze formation mechanisms based on aerosol hygroscopicity and effective density measurements

Yuanyuan Xie, Xingnan Ye*, Zhen Ma, Ye Tao, Ruyu Wang, Ci Zhang, Xin Yang, Jianmin Chen, Hong Chen

Shanghai Key Laboratory of Atmospheric Particle Pollution and Prevention (LAP$^3$), Department of Environmental Science and Engineering, Fudan University, Shanghai 200433, China.

*Correspondence to: Xingnan Ye (yexingnan@fudan.edu.cn), Jianmin Chen (jmchen@fudan.edu.cn).

**Abstract**: We characterize a representative haze event from a series of periodic particulate matter (PM) episodes that occurred in Shanghai during winter 2014. Particle size distribution, hygroscopicity, and effective density were measured online, along with analysis of water-soluble inorganic ions and single particle mass spectrometry. Regardless of pollution level, the mass ratio of SNA/$PM_{1.0}$ (sulfate, nitrate, and ammonium) slightly fluctuated around 0.28 over the whole observation, suggesting that both secondary inorganic compounds and carbonaceous aerosols (including soot and organic matter) contributed substantially to the haze formation. Nitrate was the most abundant ionic species during hazy periods, indicating that $NO_x$ contributed more to haze formation in Shanghai than did $SO_2$. The calculated PM concentration from particle size distribution displayed a variation pattern similar to that of measured

Atmos. Chem. Phys. Discuss., doi:10.5194/acp-2017-16, 2017
Manuscript under review for journal Atmos. Chem. Phys.
Discussion started: 16 February 2017


Atmospheric Chemistry and Physics Discussions

$PM_{1.0}$ during the representative PM episode, indicating that enhanced pollution level was attributable to the elevated number of larger particles. The number fraction of the near-hydrophobic group increased as the PM episode developed, indicating accumulation of local emissions. Three "banana-shape" particle evolutions were consistent with the rapid increase in $PM_{1.0}$ mass loading, indicating rapid size growth by condensation of condensable materials was responsible for the severe haze formation. Both hygroscopicity and effective density of the particles increased considerably with growing particle size during the banana-shaped evolutions, indicating that secondary transformation of $NO_x$ and $SO_2$ was a major contributor to the particle growth. Our results suggest that the accumulation of gas-phase and particulate pollutants under stagnant meteorological conditions and subsequent rapid particle growth by secondary processes, were primarily responsible for the haze pollution in Shanghai during wintertime.

**Keywords**: air pollution; size distribution; hygroscopic growth; secondary process; Shanghai.

## 1. Introduction

Atmospheric aerosol has significant influences on radiation balance and climate forcing of the atmosphere (Wang et al., 2011;Wang et al., 2014c;Wu et al., 2016a;IPCC, 2013); as well as strong impacts on visibility (Yang et al., 2012;Lin et al., 2014;Xiao et al., 2014) and public health (Heal et al., 2012) in heavily polluted areas. Recent studies found that short-term exposure to haze pollution could cause airway inflammation and aggravate respiratory symptoms in chronic obstructive pulmonary disease patients (Wu



et al., 2016b;Guan et al., 2016).

With the huge achievements in economic development and rapid urbanization over the past 30 years, particulate pollution has become a major environmental concern in China. The most severe haze event that occurred in the first quarter of 2013, spread over 1.6 million $km^2$ (Wang et al., 2014a). This event motivated the release of the Action Plan on Prevention and Control of Air Pollution with the goal of reducing $PM_{2.5}$ (particulate matter smaller than 2.5 μm in aerodynamic diameter) concentration by 15–25% in 2017 against 2012 in three major city clusters (http://english.mep.gov.cn/News_service/infocus/201309/t20130924_260707.htm). In order to reduce the $PM_{2.5}$ concentration, extensive studies have been conducted to investigate the sources and formation mechanisms of haze pollution in recent years (Ye et al., 2011;Sun et al., 2016;Qiao et al., 2016;Hu et al., 2016;Li et al., 2016;Guo et al., 2014;Zheng et al., 2015;Guo et al., 2013;Wang et al., 2016;Peng et al., 2016). However, the haze formation mechanisms and source appointment of fine particles remain uncertain.

Guo et al. (2013) summarized historical reports from 2000 to 2008 in Beijing and found that the origins of urban fine particles varied in different seasons: the contribution of primary emissions is comparable to that of secondary formation during winter heating periods whereas secondarily produced aerosols dominate the fine PM sources in other seasons. As an important type of primary emissions in urban area, black carbon (BC) is primarily from incomplete fossil fuel combustion. Light absorption of

Atmos. Chem. Phys. Discuss., doi:10.5194/acp-2017-16, 2017
Manuscript under review for journal Atmos. Chem. Phys.
Discussion started: 16 February 2017




BC aerosols is increased after atmospheric aging by coating with secondary materials and restructuring (Khalizov et al., 2009). Due to cooling effect at the surface and warming effect aloft, the enhanced light absorption and scattering by aged BC particles stabilize the atmosphere, hindering vertical transport of gaseous and particulate pollutants (Wang et al., 2013). BC aging occurs much more efficiently in the presence of highly elevated gaseous aerosol precursors so that light absorption increases by a factor of 2.4 within 4.6 h under highly polluted conditions in Beijing, significantly exacerbating pollution accumulation and strongly contributing to severe haze formation (Peng et al., 2016).

Due to the implement of several effective regulatory policies, the increasing trend of primary emissions has been under control since the 11$^{th}$ five-year period. A growing number of studies suggested that secondary production was the major contributor to the haze episodes in recent years (Shi et al., 2014;Zhao et al., 2013;Zhang et al., 2015a;Huang et al., 2014), in contrast that primary emissions were of great importance in some haze episodes (Niu et al., 2016). Guo et al. (2014) reported that the development of PM episodes in Beijing was characterized by efficient nucleation and continuous particle growth over an extend period dominated by local secondary formation. They attributed the continuous growth of particle size and constant accumulation of particle mass concentration to the highly elevated concentrations of gaseous precursors such as $NO_x$, $SO_2$, and volatile organic compounds (VOCs), while the contribution from primary emissions and regional transport was negligible. However, the role of regional transport of $PM_{2.5}$ in haze formation remains controversial (Li et al., 2015;Zhang et al., 2015b).

Atmos. Chem. Phys. Discuss., doi:10.5194/acp-2017-16, 2017
Manuscript under review for journal Atmos. Chem. Phys.
Discussion started: 16 February 2017




The most important advances in the understanding of urban PM formation were reviewed by Zhang et al. (2015c). The concentrations of $SO_2$, $NO_x$, and anthropogenic source VOCs in Beijing and other cities of the developing world are significantly higher than those in the urban areas of developed countries, resulting in large secondary production of sulfate, nitrate, and SOA. Synergetic effects among various organic and inorganic compounds may exist under highly polluted conditions, indicating different PM formation rates between developing and developed urban regions. Indeed, a large enhancement of particulate sulfate was typically observed during regional haze events in China (Chen et al., 2016;Wang et al., 2015;Fu et al., 2008;Xie et al., 2015). Currently, the highly elevated sulfate concentration during haze episodes cannot be fully explained by model simulations (Wang et al., 2014b;Chen et al., 2016). Recently, a significant breakthrough made by Wang et al. (2016) has provided a reasonable explanation in the high level of sulfate during haze episodes. It is revealed by their laboratory experiments that aqueous oxidation of $SO_2$ by $NO_2$ proceeds more efficiently with the increase of $NO_2$ concentration whereas the reaction is suppressed in acid conditions, because acid effect reduces the solubility of $SO_2$ and reaction rate. The enhanced sulfate formation during severe haze periods in Beijing was attributable to aqueous oxidation of $SO_2$ by $NO_2$ on hygroscopic fine particles under conditions of elevated RH and the concentrations of $NH_3$ and $NO_2$, which was confirmed by the comparable $SO_2$ uptake coefficients for sulfate formation from field and laboratory results.

The hygroscopic properties of ambient particles vary significantly depending on the origin of the air



masses and the atmospheric aging process. In urban air, the population of near-hydrophobic particles can be assumed to consist largely of freshly emitted combustion particles containing high mass fractions of soot and water-insoluble organic compounds (Swietlicki et al., 2008;Massling et al., 2009). In contrast, secondary sulfate or nitrate aged particles are more-hygroscopic, and their relative abundance is primarily responsible for the hygroscopic growth of ambient particles at elevated RH (Topping et al., 2005;Aggarwal et al., 2007;Gysel et al., 2007). Thus, hygroscopicity can serve as a tracer of source origins, mixing state, and aging mechanisms of ambient particles. For example, temporal variations of aerosol hygroscopicity have helped the explanation of haze formation mechanisms in Beijing and Shanghai (Ye et al., 2011;Guo et al., 2014).

Density is one of the most important physicochemical properties for atmospheric aerosols. Effective density has served as a tracer for new particle formation and for the aging process in previous studies (Yin et al., 2015;Guo et al., 2014). The ambient particles in urban areas are mostly complex mixtures of elemental carbon (EC), organics (OC), and secondary inorganic aerosols (SIA) (Hu et al., 2012). The effective densities of traffic particles are below 1.0 g $cm^{-3}$, and density decreases with the increase of particle size because there are more voids between primary particles in relatively larger aggregates (Momenimovahed and Olfert, 2015). The density of OC is in between those of EC and SIA, and varies with source. The effective density of combustion particles increases by filling the voids in the agglomerate particles with condensed semi-volatile materials, or by restructuring agglomerates with hygroscopic SIA

Atmos. Chem. Phys. Discuss., doi:10.5194/acp-2017-16, 2017
Manuscript under review for journal Atmos. Chem. Phys.
Discussion started: 16 February 2017




(Momenimovahed and Olfert, 2015;Zhang et al., 2008).

In this study, a combined HTDMA-APM system was used to investigate the variations of hygroscopicity and effective density of submicrometer aerosols during winter 2014 in urban Shanghai. In addition, cascade samples were collected and a single particle mass spectrometry was used to better understand the hygroscopicity and density variations. The primary objectives of this study were to investigate the particle growth mechanisms and to identify the contribution of local emissions during the winter haze episode.

## 2. Experimental

### 2.1. Sampling site

The measurements were conducted from December 21, 2014 to January 13, 2015 at the Department of Environmental Science and Engineering in the main campus of Fudan University (31.30°N, 121.5°E), a representative urban site close to a sub-center of Shanghai (Ye et al., 2010). At a supersite about 100 m away, $PM_{1.0}$ was monitored using a Thermo Scientific™ 5030 SHARP monitor. Trace gas pollutants were monitored using Thermo Scientific™ i-series gas analyzers (43i for $SO_2$, 49i for $O_3$, 42i for $NO/NO_2/NO_x$), and meteorological data were monitored using an automatic meteorological station (Model CAWS600, Huayun Inc., China) (Yin et al., 2015). The concentrations of $PM_{2.5}$, $PM_{10}$, and CO were released by the Shanghai Environmental Monitoring Center. The height of the Planet Boundary Layer (PBL) was



126 computed online using the NCEP Global Data Assimilation System (GDAS) model
127 (http://ready.arl.noaa.gov/READYamet.php).

128 **2.2. HTDMA-APM system**

129 Particle size distribution, hygroscopic growth factor (GF), and effective density were measured using
130 a custom-built HTDMA-APM system (Figure 1). The custom-built HTDMA (Hygroscopic Tandem
131 Differential Mobility Analyzers) mainly consist of two long DMAs (3081L, TSI Inc.), a humidifier (PD-
132 50T-12MSS, Perma Pure Inc.) and a Condensation Particle Counter (CPC, Model 3771, TSI Inc.). A
133 detailed description of the HTDMA is available in Ye et al. (2009). In this observation, particle number
134 size distribution in the range of 14–600 nm and hygroscopic growth at 83% RH for particles with dry
135 diameters of 40, 100, 220, 300, 350, and 400 nm were determined by HTDMA (in turn). The
136 determination of effective density by DMA-APM was described previously (Yin et al., 2015;Pagels et al.,
137 2009). Briefly, a combined system consisting of a compact Aerosol Particle Mass Analyzer (APM, Model
138 3601, Kanomax Inc.) and a CPC (Model 3775, TSI Inc.) was connected to the sample tubing through a
139 3-way electrical switch behind the upstream DMA (DMA1). The APM comprises two coaxial cylindrical
140 electrodes rotating at the same angular velocity. Charged aerosol particles of a certain diameter sized by
141 DMA1 are axially fed into the annular gap between the electrodes and experienced an outward centrifugal
142 force from the particle rotating and an inward electrostatic force from the high-voltage field between the
143 electrodes. Particles pass through the APM and are sent to the CPC when the two forces are balanced.

Atmos. Chem. Phys. Discuss., doi:10.5194/acp-2017-16, 2017
Manuscript under review for journal Atmos. Chem. Phys.
Discussion started: 16 February 2017


Atmospheric Chemistry and Physics Discussions

144 The mass of particles that pass through the APM is determined by the rotation rate and the applied voltage.
145 Effective densities for dry diameters of 40, 100, 220, and 300 nm were determined by the method of
146 DMA-APM in this study. The HTDMA-APM was operated alternatively in HTDMA mode and then
147 DMA-APM mode, for every 40 min.

148 Before the field observation, the HTDMA-APM was calibrated using 40–450 nm NIST-Traceable PSL
149 particles and ammonium sulfate. The measured HTDMA data were inversed with the $TDMA_{inv}$ algorithm
150 to obtain the actual GF distribution. This is because the raw data are only a skewed and smoothed
151 integral transform of the actual growth factor probability density function (GF-PDF) (Gysel et al., 2009).
152 The hygroscopicity parameter κ was derived from the GF data after inversion with the $TDMA_{inv}$ algorithm
153 according to the κ-Köhler theory (Petters and Kreidenweis, 2007).

154 **2.3. SPAMS**

155 A Single Particle Aerosol Mass Spectrometry (SPAMS, Hexin Analytical Instrument Co., Ltd., China)
156 installed in the same room with the HTDMA-APM system was used to obtain the chemical and size
157 information of individual particles in the range of 0.2-2 μm. Detailed information on SPAMS is available
158 in Li et al. (2011). Briefly, ambient particles are drawn into a vacuum chamber through an aerodynamic
159 focusing lens and accelerated to a size-dependent terminal velocity. Sized particles are desorbed and
160 ionized by the pulsed desorption/ionization laser (Q-switched Nd: YAG, λ=266 nm) at the ion source
161 region. Both positive and negative mass spectra for a single particle are recorded by a bipolar time-of-



flight spectrometer. The single particle information was imported into YAADA (version 2.11, www.yaada.org). Based on the similarities of the mass-to-charge ratio and peak intensity, particles were classified using the ART-2a method.

### 2.4. Ion chromatography

Cascade aerosol samples for offline analysis were collected at the roof platform of the Environmental Building using a 10-stage MOUDI sampler (Micro-Orifice Uniform Deposit Impactor, Model 110-NR, MSP Corp., USA). Detailed description of the sampling, pretreatment, chemical analysis, and quality control of this system is available in Tao et al. (2016). Briefly, cascade samples were collected every 24 h using the PALL7204 quartz filter as the collection substrate. Each filter was weighted with a BP211D electronic balance at 25±1°C and 40±2%RH. The water extract of each sample was analyzed using an Ion Chromatograph (Metrohm 883 basic IC plus, Switzerland) equipped with a third-party column heater (CT-100, Agela Corp., China). Seven anions ($F^-$, $Cl^-$, $NO_2^-$, $Br^-$, $NO_3^-$, $SO_4^{2-}$ and $PO_4^{3-}$) were resolved using a Metrosep A Supp 5-250/4.0 column at 35°C with an eluent of 3.2 mmol $L^{-1}$ $Na_2CO_3$ + 1.0 mmol $L^{-1}$ $NaHCO_3$. Six cations ($Li^+$, $Na^+$, $NH_4^+$, $K^+$, $Ca^{2+}$, and $Mg^{2+}$) were separated by a Metrosep C4-250/4.0 column at 30°C with an eluent of 1.7 mmol $L^{-1}$ $HNO_3$ + 0.7 mmol $L^{-1}$ 2,6-pyridine dicarboxylic acid.

## 3. Results and discussion

### 3.1. Periodic cycle of PM episodes during the observation period

Atmos. Chem. Phys. Discuss., doi:10.5194/acp-2017-16, 2017
Manuscript under review for journal Atmos. Chem. Phys.
Discussion started: 16 February 2017


Atmospheric Chemistry and Physics Discussions

Figure 2 shows the temporal variations of PM mass loading during the winter observation (December 21, 2014 to January 13, 2015). The official data of $PM_{2.5}$ and $PM_{10}$ were blank on some clean days. Meteorologically, our measurement was deployed in a typical winter period. The average concentrations of $PM_{1.0}$, $PM_{2.5}$, and $PM_{10}$ were 57.3±37.0, 87.2±67.2, and 127.8±77.7 μg $m^{-3}$, respectively. About 62% of hourly averaged $PM_{2.5}$ concentrations exceeded 75 μg $m^{-3}$ of the Chinese Grade II guideline (GB 3095-2012), indicating heavy particle pollution in Shanghai during wintertime. The PM episodes exhibited a clear periodic cycle of ~5 days. A similar feature was previously observed in Beijing (Guo et al., 2014). At the beginning of each cycle, the $PM_{1.0}$ level was below 35 μg $m^{-3}$. During the clean period, the differences among the concentrations of $PM_{1.0}$, $PM_{2.5}$, and $PM_{10}$ were insignificant. Occasionally the measured $PM_{2.5}$ concentrations were larger than those of $PM_{10}$, possibly due to system error. However, the particle mass concentration began to increase in the next few days, with $PM_{1.0}$ and $PM_{2.5}$ peaking at over 100 and 200 μg $m^{-3}$, respectively. During the late episodes, the PM mass loading abruptly dropped, due to change in the atmospheric dilution or wet deposition.

### 3.2 Contributions of secondary inorganic aerosols to $PM_{1.0}$ mass loading

Figure 3 illustrates the daily concentrations of sulfate, nitrate, and ammonium as a function of $PM_{1.0}$ mass loading. In general, the sum of concentrations of sulfate, nitrate, and ammonium (SNA) increased linearly as $PM_{1.0}$ mass loading increased. It is noticeable that the SNA/$PM_{1.0}$ ratio slightly fluctuated around 0.28, regardless of the pollution level. Because soil dust and sea salt made a negligible contribution

Atmos. Chem. Phys. Discuss., doi:10.5194/acp-2017-16, 2017
Manuscript under review for journal Atmos. Chem. Phys.
Discussion started: 16 February 2017


Atmospheric Chemistry and Physics Discussions

198 to the fine particle mass concentration in this study, the almost constant ratio of SNA/$PM_{1.0}$ indicates that
199 SNA and carbonaceous aerosols (including soot and organic matter) synchronously increased during haze
200 episodes. As the $PM_{1.0}$ concentration increased, the concentration of nitrate increased more rapidly than
201 sulfate so that it became the most abundant ionic species at $PM_{1.0}$ > 40 μg $m^{-3}$. This indicated that $NO_x$
202 contributed more to haze formation in Shanghai than did coal-fired sources. Generally, the visibility
203 decreased with the increase in PM concentration, indicating photochemical activity began to weaken as
204 the development of haze episodes. The large increase in nitrate concentration may be attributable to
205 heterogeneous reaction on the preexisting particles. Nitrate formation is highly dependent on the surface
206 area of preexisting particles and is favored under $NH_3$-rich conditions (Chu et al., 2016). In contrast, Han
207 et al. (2016) reported that the mass ratio of nitrate to sulfate decreased with increase of $PM_{2.5}$ level and
208 that the sources of sulfate contributed more to haze formation in Beijing than mobile sources. This finding
209 suggests that the haze formation mechanism is likely different in Shanghai and Beijing. VOCs and $NO_x$
210 are exclusively from local emissions whereas regional transport is a big source of $SO_2$ under stagnant
211 atmosphere, due to their different atmospheric lifetimes (Guo et al., 2014). Considering the relatively
212 smaller contribution of sulfate, our results reveal that the accumulation and secondary transformation of
213 local emissions likely played a dominant role in this haze formation.

214 **3.3 Aerosol hygroscopicity and effective density during the observation period**

215 Figure 4a displays a box chart of the median hygroscopicity of each hygroscopic growth factor



distribution for different sizes. Considering all of the growth factor distributions collectively, the hygroscopicity parameter κ increased with increase of the dry diameter, with an average κ of 0.161 at 40 nm and 0.338 at 300 nm. Assuming a two-component system of a model salt (ammonium sulfate, $\kappa_m$ = 0.53) and an insoluble species (κ = 0), the volume fraction of hygroscopic species (ε) can be obtained based on the Zdanovsldi-Stokes-Robinson (ZSR) mixing rule. The average ε was 0.3 for 40 nm particles, suggesting that the primary particles or initial growth of freshly generated particles were dominated by non-hygroscopic species. In contrast, the 300 nm particles were extremely aged, with more-hygroscopic species.

Generally, the HTDMA-measured hygroscopicity was limited to the size range below 250 nm, and it is common that the GF increases with increase of particle size. The increase of aerosol hygroscopicity with size was attributed to the addition of more-hygroscopic SNA (Swietlicki et al., 2008;Ye et al., 2010). Gasparini et al. (2006) reported that the GF first increased and then decreased with increase of particle size, peaking at the diameter of 300 nm. In this study, the determination size range was extended to 400 nm and no decrease in GF was observed. We attribute the different hygroscopicity to the large emissions of $SO_2$ and $NO_x$ in China, which were responsible for the strong formation of sulfate and nitrate. The variation of hygroscopicity parameter κ was much greater for 40 nm particles. The particle population with κ < 0.1 was attributed to fresh traffic particles (Ye et al., 2013). The considerable percentile of κ < 0.1 indicated that the 40 nm particle population was sometimes dominated by near-hydrophobic particles.

Atmos. Chem. Phys. Discuss., doi:10.5194/acp-2017-16, 2017
Manuscript under review for journal Atmos. Chem. Phys.
Discussion started: 16 February 2017


Atmospheric Chemistry and Physics Discussions

Figure 4b displays a box chart of median effective density for different particle sizes. The median effective density varied in the narrow range of $\rho_{eff}$ = 1.35–1.41 g cm$^{-3}$ for 40–300 nm particle population. The size distribution of particle density varied in the literature. Hu et al. (2012) and Yin et al. (2015) reported that particle density increased as particle size increased while a contradictory trend was observed by Geller et al. (2006) and Spencer et al. (2007). The difference was attributable to the contribution of fresh traffic particles. Although the dominant accumulation mode particles have an effective density greater than Aitken mode ones, the presence of a lower effective density group associated with emissions from traffic exhaust might decrease the mean effective density to a value lower than that of Aitken mode particles (Levy et al., 2014). Yin et al. (2015) reported that a quasi-monodisperse density distribution was dominant for accumulation mode particles. In contrast, externally mixed aerosols with a lower density group ($\rho_{eff}$ = ~1.0 g cm$^{-3}$) were often present in this observation, and were responsible for the decrease of the mean effective density. The lower effective density group was attributed to fresh or slightly aged traffic-related particles, because the number fraction of the lower density group increased as the concentration of NO increased.

### 3.4 Characteristics of a representative PM episode

The PM episode from January 7 to 12 was a representative case of severe haze formation and elimination processes. It can be divided into clean (January 7), transition (January 8), haze (January 9–11), and post-haze (January 12) periods. During the transition from the clean to haze period (January 7 to 8),

Atmos. Chem. Phys. Discuss., doi:10.5194/acp-2017-16, 2017
Manuscript under review for journal Atmos. Chem. Phys.
Discussion started: 16 February 2017


Atmospheric Chemistry and Physics Discussions

both $PM_{1.0}$ and $PM_{2.5}$ concentrations increased slightly, with an average $PM_{1.0}/PM_{2.5}$ ratio of 0.65. A sharp increase in $PM_{2.5}$ (of 125 μg $m^{-3}$) was observed from 6:00 to 12:00 local time on the morning of January 9. During the haze period, the concentration of $PM_{2.5}$ exceeded 115 μg $m^{-3}$ (medially polluted level, HJ633-2012) for 63 h. On January 11, the hourly $PM_{2.5}$ concentration exceeded 250 μg $m^{-3}$, corresponding to the severely polluted level.

Figure 5 displays the temporal evolution of particle size distribution in comparison with the measured $PM_{1.0}$ concentration during the representative PM episode. The calculated PM concentrations ($PM_{cal}$) were obtained based on the particle size distribution and average effective density of 1.39 g $m^{-3}$ in the range of 14–600 nm measured in this study. In contrast to the fact that particle size distribution was dominated by nanoparticles during the clean period, the burst of Aitken mode particles and subsequent continuous growth to approximately 200 nm in diameter was observed three times during the haze period, indicating that the presence of numerous larger particles is likely responsible for the severe particle pollution (Guo et al., 2014). The importance of larger particles in haze formation is also illustrated by the contour plot of the particle volume size distribution. The difference of total number concentration between transition and haze periods was insignificant, whereas the volume concentration increased rapidly during the haze period. This feature clearly demonstrates that the haze formation was closely correlated with particle growth and elevated number of larger particles.

Interestingly, the particle mass concentration was sensitive to variations of wind speed and planetary

Atmos. Chem. Phys. Discuss., doi:10.5194/acp-2017-16, 2017
Manuscript under review for journal Atmos. Chem. Phys.
Discussion started: 16 February 2017




boundary layer (PBL). During the transition and haze periods, the wind speed decreased considerably with insignificant change in prevailing wind (Figure S1). This indicated that outside transportation became less and less significant. It is noteworthy that the temporal evolution of the particle mass concentration was inversely correlated with the PBL height. The decreasing PBL provided a stagnant atmosphere that favored the accumulation of local emissions. This finding reveals that the severe haze pollution was likely triggered by the adverse meteorological conditions. The impact of decreasing PBL height on haze formation can also be evidenced by the variations of trace gaseous species (Figure S2). During the PM episode, the concentrations of $NO_2$, $SO_2$, and CO displayed variation trends similar to that of the particle concentration. The fluctuations of trace gas concentrations were caused by primary emission and secondary processes. Noticeably, the concentration of NO increased dramatically in rush hours during the haze period, whereas it fluctuated slightly during the clean period; indicating that local emissions were easily accumulated under stagnant atmosphere. In addition, the maximum concentration of $O_3$ remained considerably higher during daytime, whereas it decreased significantly at night. The most plausible explanation is that $O_3$ was consumed rapidly by the accumulating trace gases, such as $NO_x$, and VOCs.

### 3.5 Variations of hygroscopicity and effective density during the PM episode

Figure 6 shows the averaged hygroscopicity and effective density for different pollution periods of the PM episode. Regardless of the pollution period, near- hydrophobic particles were externally mixed with



some hygroscopic particles. During the clean period, the more-hygroscopic particles dominated the 40 nm particle population, indicating that the near-hydrophobic primary particles were rapidly dispersed due to atmospheric dilution. The number fraction of the near-hydrophobic group for different sizes increased as the PM episode developed, indicative of the increasing accumulation of local emissions. Notably, the increase of the near-hydrophobic particles with the evolution of the PM episode become less significant as particle size increased, indicating that primary emission exerted a more significant impact on smaller particles than on larger ones. The median diameter of nascent traffic particles from various gasoline sources ranged between 55 and 73 nm with an average of 65 nm (Momenimovahed and Olfert, 2015). Therefore, the number fraction of the near-hydrophobic particles larger than 200 nm is not sensitive to the accumulation of traffic emissions.

Interestingly, the variations of particle effective density for different sizes are in good agreement with the hygroscopicity. The dominant peak of effective density distribution appeared at $\rho_{eff}$ = ~1.5 g cm$^{-3}$ for 40 nm particles in the clean period, indicating that they are highly aged with hygroscopic inorganic salts (Yin et al., 2015). As the episode developed, the mean density shifted to lower values, indicating the increasing contribution of less-massive carbonaceous materials. The averaged density distribution was broadened as the episode developed, suggesting that it could be deconvolved into two groups and that the number fraction of the low-density group increased. This finding revealed that the less-massive particles are less hygroscopic whereas the larger density group corresponds to the more-hygroscopic one. In



addition, the variations of hygroscopicity and effective density coincided with the evolution of PBL height, indicating that the increasing accumulation of local emissions due to adverse atmospheric conditions is likely responsible for the enhancement of those near-hydrophobic and less-massive particles.

Figure 7 displays the temporal profiles for contributions of EC (including bare EC and OC-coated EC), OC, sulfate, and nitrate determined by SPAMS. Obviously, the relative contribution of nitrate increased as the episode developed. In contrast, the relative contribution of sulfate displayed an opposite trend. This feature is comparable with the aforementioned results of SNA, thus further highlighting the important role of nitrate in haze formation in Shanghai. The number fraction of EC particles generally increased during the haze period, peaking at midnight on January 9 and 10. It should be pointed out that the measured number fraction possibly underestimated the contribution of EC particles because the dominant size range of fresh traffic particles is below the detection limit of SPAMS (0.2–2.0 μm). This finding provides good support for the increase of near-hydrophobic and less-dense particles as the episode developed. Niu et al. (2016) reported that the number ratio of secondary particles to soot in haze samples was higher than that collected in the clean days in Beijing. Our finding is comparable to their results. In contrast, the number fraction of pure OC decreased during the pollution event. The possible explanation is that the condensation of organic matter was favored on the large amount of preexisting EC particles, or that photo-oxidation of VOCs was minimized due to lower solar radiation.

### 3.6 Evolutions of hygroscopicity and effective density with particle growth

Atmos. Chem. Phys. Discuss., doi:10.5194/acp-2017-16, 2017
Manuscript under review for journal Atmos. Chem. Phys.
Discussion started: 16 February 2017


Atmospheric Chemistry and Physics Discussions

Three "banana-shape" evolutions of the particle size distribution were identified in the representative PM episode. The banana-type contour plot of particle size distributions is a typical characteristics of new particle formation (NPF) events and traditionally regarded as one of the most important criteria for identifying NPF (Xiao et al., 2015;Dal Maso et al., 2005;Levy et al., 2013;Zhang et al., 2012). Atmospheric NPF is often defined by the burst of nucleation mode particles and subsequent growth of the nuclei to larger particles (Zhang et al., 2012;Kulmala et al., 2012). Gas-phase sulfuric acid produced via oxidation of $SO_2$ by OH radical plays a dominant role in the NPF events. NPF is typically completely suppressed when preexisting particles is abundant, because gas-phase sulfuric acid is rapidly lost to the surfaces of preexisting aerosols (Zhang et al., 2012). In addition to sulfuric acid, low-volatility organic species, and interaction between sulfate and organics are important for NPF (Zhang et al., 2004;Zhao et al., 2009). However, the possibility of NPF can be ignored in this study due to the absence of the burst of nucleation mode particles and the high concentration of $PM_{1.0}$. The burst of Aitken mode particles was attributable to rapid accumulation of traffic emissions during rush hours under stagnant atmospheric conditions. The ''banana-shape'' evolutions were primarily caused by coagulation and condensation growth, which provided an excellent opportunity to reveal the chemical mechanism of particle growth during the PM episode.

The first "banana-shape'' evolution of the particle size distribution occurred from approximately 05:00 to 15:00 on January 9, with increase of the particle number concentration ($N_{total}$) from $1.7\times10^4$ to $3.4\times10^4$



342 $cm^{-3}$ followed by a decrease trend until 17:00 (Period 1). The second ‘‘banana-shape’’ evolution occurred
343 from approximately 18:00 on January 9 to approximately 12:00 on January 10 (Period 2). The $N_{total}$
344 increased from $2.1\times10^4$ to $4.2\times10^4$ $cm^{-3}$ within 3 h, followed by gradual decrease of $N_{total}$ in contrast to
345 continuous increase of the particle mass concentration. During the growth process, the mode diameter of
346 the particle population increased from below 40 nm to approximately 200 nm. The third “banana-shape”
347 evolution began in the evening rush hours on January 10, with continuous increase of PM mass
348 concentration for 12 h (Period 3).

349 Figure 8 illustrates the evolution of particle hygroscopicity and effective density during periods 2 and
350 3. During the initial stage, the measured GF and effective density distributions were both bimodal, with
351 a dominant peak at GF = ~1.0 and $\rho_{eff}$ = ~1.0 g $cm^{-3}$, respectively. In a previous study, we found that the
352 number fraction of near-hydrophobic particles varied with the traffic exhaust (Ye et al., 2013). Moreover,
353 laboratory studies showed that the effective density of 50 nm vehicle particles was approximately 1.0 g
354 $cm^{-3}$ (Olfert et al., 2007;Park et al., 2003;Momenimovahed and Olfert, 2015). These findings indicate that
355 the initial burst of Aitken mode particles is attributable to the presence of enhanced traffic-related
356 emissions. In contrast, the number fraction and GF of the more-hygroscopic group increased with growing
357 particle size, indicating the addition of hygroscopic inorganic species. The variation of the effective
358 density of the particles was similar to that of the hygroscopicity, indicating the increase of high density
359 materials. In general, inorganic sulfate and nitrate are more hygroscopic and denser than soot particles or

Atmos. Chem. Phys. Discuss., doi:10.5194/acp-2017-16, 2017
Manuscript under review for journal Atmos. Chem. Phys.
Discussion started: 16 February 2017




organic aerosols (Yin et al., 2015). These findings suggest that secondary sulfate and nitrate increased with the growing particle size, indicating the importance of the conversion of $SO_2$ and $NO_x$ in particle growth. This conclusion is supported by the largest SNA concentration in $PM_{1.0}$ during the PM episode (31.3 μg $m^{-3}$ on January 10 and 23.8 μg $m^{-3}$ on January 11). Considering that the concentration of nitrate was much higher than that of sulfate during the haze event, the increase of hygroscopicity was dominated by the addition of nitrate.

## 4. Conclusions

Particle size distribution, size-resolved hygroscopic growth and effective density of sub-micrometer aerosols were determined using a HTDMA-APM system along with measurements of cascade samples and single particle mass spectrometry in urban Shanghai during winter 2014.

The PM episode exhibited a periodic cycle of ~5 days. The average concentration of $PM_{2.5}$ was 87.2±67.2 μg $m^{-3}$, with approximately 62% of hourly $PM_{2.5}$ concentrations exceeding the Chinese Grade II guideline. Both secondary inorganic salts and carbonaceous aerosols contributed substantially to haze formation, because the SNA/$PM_{1.0}$ ratio was almost constant during the observation period. Nitrate became the most abundant ionic species at $PM_{1.0}$ >40 μg $m^{-3}$, indicating that the sources of nitrate contributed more to haze formation in Shanghai than did $SO_2$.

The severe haze pollution was likely triggered by the adverse meteorological conditions, which caused



a large accumulation of local emissions and subsequent rapid growth to larger particles. As the PM episode developed, the number fraction of near-hydrophobic particles of different size increased, consistent with decrease of the mean effective density. Both hygroscopicity and effective density of the particles were found to increase considerably with growing particle size, indicating that secondary aerosol formation was a major contributor to particle growth. Our results suggest that the accumulation of local emissions under adverse meteorological conditions and subsequent rapid particle growth by secondary processes are primarily responsible for the haze pollution in Shanghai during wintertime.

**Acknowledgments**

This work was supported by the National Natural Science Foundation of China (21477020, 21527814, and 91544224), and the National Science and Technology Support Program of China (2014BAC22B01).

Reference

Aggarwal, S. G., Mochida, M., Kitamori, Y., and Kawamura, K.: Chemical closure study on hygroscopic properties of urban aerosol particles in Sapporo, Japan, Environmental Science & Technology, 41, 6920-6925, 10.1021/es063092m, 2007.

Chen, D., Liu, Z., Fast, J., and Ban, J.: Simulations of sulfate-nitrate-ammonium (SNA) aerosols during the extreme haze events over northern China in October 2014, Atmospheric Chemistry and Physics, 16,

396 10707-10724, 10.5194/acp-16-10707-2016, 2016.

397 Chu, B., Zhang, X., Liu, Y., He, H., Sun, Y., Jiang, J., Li, J., and Hao, J.: Synergetic formation of secondary
398 inorganic and organic aerosol: effect of SO2 and NH3 on particle formation and growth, Atmospheric
399 Chemistry and Physics, 16, 14219-14230, 10.5194/acp-16-14219-2016, 2016.

400 Dal Maso, M., Kulmala, M., Riipinen, I., Wagner, R., Hussein, T., Aalto, P. P., and Lehtinen, K. E. J.:
401 Formation and growth of fresh atmospheric aerosols: eight years of aerosol size distribution data from
402 SMEAR II, Hyytiala, Finland, Boreal Environment Research, 10, 323-336, 2005.

403 Fu, Q. Y., Zhuang, G. S., Wang, J., Xu, C., Huang, K., Li, J., Hou, B., Lu, T., and Streets, D. G.:
404 Mechanism of formation of the heaviest pollution episode ever recorded in the Yangtze River Delta, China,
405 Atmospheric Environment, 42, 2023-2036, 2008.

406 Gasparini, R., Li, R. J., Collins, D. R., Ferrare, R. A., and Brackett, V. G.: Application of aerosol
407 hygroscopicity measured at the Atmospheric Radiation Measurement Program's Southern Great Plains
408 site to examine composition and evolution, J. Geophys. Res.-Atmos., 111, D05S12,
409 doi:10.1029/2004JD005448, 10.1029/2004jd005448, 2006.

410 Guan, W. J., Zheng, X. Y., Chung, K. F., and Zhong, N. S.: Impact of air pollution on the burden of chronic
411 respiratory diseases in China: time for urgent action, Lancet, 388, 1939-1951, 2016.

412 Guo, S., Hu, M., Guo, Q., Zhang, X., Schauer, J. J., and Zhang, R.: Quantitative evaluation of emission
413 controls on primary and secondary organic aerosol sources during Beijing 2008 Olympics, Atmospheric

414 Chemistry and Physics, 13, 8303-8314, 10.5194/acp-13-8303-2013, 2013.

415 Guo, S., Hu, M., Zamora, M. L., Peng, J., Shang, D., Zheng, J., Du, Z., Wu, Z., Shao, M., Zeng, L., Molina,

416 M. J., and Zhang, R.: Elucidating severe urban haze formation in China, Proceedings of the National

417 Academy of Sciences of the United States of America, 111, 17373-17378, 10.1073/pnas.1419604111,

418 2014.

419 Gysel, M., Crosier, J., Topping, D. O., Whitehead, J. D., Bower, K. N., Cubison, M. J., Williams, P. I.,

420 Flynn, M. J., McFiggans, G. B., and Coe, H.: Closure study between chemical composition and

421 hygroscopic growth of aerosol particles during TORCH2, Atmospheric Chemistry and Physics, 7, 6131-

422 6144, 2007.

423 Gysel, M., McFiggans, G. B., and Coe, H.: Inversion of tandem differential mobility analyser (TDMA)

424 measurements, Journal of Aerosol Science, 40, 134-151, 10.1016/j.jaerosci.2008.07.013, 2009.

425 Han, B., Zhang, R., Yang, W., Bai, Z., Ma, Z., and Zhang, W.: Heavy haze episodes in Beijing during

426 January 2013: Inorganic ion chemistry and source analysis using highly time-resolved measurements

427 from an urban site, Science of The Total Environment, 544, 319-329,

428 http://dx.doi.org/10.1016/j.scitotenv.2015.10.053, 2016.

429 Heal, M. R., Kumar, P., and Harrison, R. M.: Particles, air quality, policy and health, Chemical Society

430 Reviews, 41, 6606-6630, 10.1039/c2cs35076a, 2012.

431 Hu, M., Peng, J., Sun, K., Yue, D., Guo, S., Wiedensohler, A., and Wu, Z.: Estimation of size-resolved



ambient particle density based on the measurement of aerosol number, mass, and chemical size distributions in the winter in Beijing, Environ Sci Technol, 46, 9941-9947, 10.1021/es204073t, 2012.

Hu, Q. Q., Fu, H. B., Wang, Z. Z., Kong, L. D., Chen, M. D., and Chen, J. M.: The variation of characteristics of individual particles during the haze evolution in the urban Shanghai atmosphere, Atmospheric Research, 181, 95-105, 10.1016/j.atmosres.2016.06.016, 2016.

Huang, R.-J., Zhang, Y., Bozzetti, C., Ho, K.-F., Cao, J.-J., Han, Y., Daellenbach, K. R., Slowik, J. G., Platt, S. M., Canonaco, F., Zotter, P., Wolf, R., Pieber, S. M., Bruns, E. A., Crippa, M., Ciarelli, G., Piazzalunga, A., Schwikowski, M., Abbaszade, G., Schnelle-Kreis, J., Zimmermann, R., An, Z., Szidat, S., Baltensperger, U., El Haddad, I., and Prevot, A. S. H.: High secondary aerosol contribution to particulate pollution during haze events in China, Nature, 514, 218-222, 10.1038/nature13774, 2014.

IPCC: Climate Change 2013: The Physical Science Basis, Cambridge, UK, 2013.

Khalizov, A. F., Xue, H., Wang, L., Zheng, J., and Zhang, R.: Enhanced Light Absorption and Scattering by Carbon Soot Aerosol Internally Mixed with Sulfuric Acid, Journal of Physical Chemistry A, 113, 1066-1074, 10.1021/jp807531n, 2009.

Kulmala, M., Petaja, T., Nieminen, T., Sipila, M., Manninen, H. E., Lehtipalo, K., Dal Maso, M., Aalto, P. P., Junninen, H., Paasonen, P., Riipinen, I., Lehtinen, K. E., Laaksonen, A., and Kerminen, V. M.: Measurement of the nucleation of atmospheric aerosol particles, Nature protocols, 7, 1651-1667, 10.1038/nprot.2012.091, 2012.

450 Levy, M. E., Zhang, R. Y., Khalizov, A. F., Zheng, J., Collins, D. R., Glen, C. R., Wang, Y., Yu, X. Y.,
451 Luke, W., Jayne, J. T., and Olaguer, E.: Measurements of submicron aerosols in Houston, Texas during
452 the 2009 SHARP field campaign, J. Geophys. Res.-Atmos., 118, 10518-10534, 10.1002/jgrd.50785, 2013.
453 Levy, M. E., Zhang, R. Y., Zheng, J., Tan, H. B., Wang, Y., Molina, L. T., Takahama, S., Russell, L. M.,
454 and Li, G. H.: Measurements of submicron aerosols at the California-Mexico border during the Cal-Mex
455 2010 field campaign, Atmospheric Environment, 88, 308-319, 10.1016/j.atmosenv.2013.08.062, 2014.
456 Li, J. J., Wang, G. H., Ren, Y. Q., Wang, J. Y., Wu, C., Han, Y. N., Zhang, L., Cheng, C. L., and Meng, J.
457 J.: Identification of chemical compositions and sources of atmospheric aerosols in Xi'an, inland China
458 during two types of haze events, Science of the Total Environment, 566, 230-237,
459 10.1016/j.scitotenv.2016.05.057, 2016.
460 Li, L., Huang, Z. X., Dong, J. G., Li, M., Gao, W., Nian, H. Q., Fu, Z., Zhang, G. H., Bi, X. H., Cheng,
461 P., and Zhou, Z.: Real time bipolar time-of-flight mass spectrometer for analyzing single aerosol particles,
462 International Journal of Mass Spectrometry, 303, 118-124, 10.1016/j.ijms.2011.01.017, 2011.
463 Li, P., Yan, R., Yu, S., Wang, S., Liu, W., and Bao, H.: Reinstate regional transport of $PM_{2.5}$ as a major
464 cause of severe haze in Beijing, Proceedings of the National Academy of Sciences of the United States of
465 America, 112, E2739-E2740, 10.1073/pnas.1502596112, 2015.
466 Lin, Y., Huang, K., Zhuang, G., Fu, J. S., Wang, Q., Liu, T., Deng, C., and Fu, Q.: A multi-year evolution
467 of aerosol chemistry impacting visibility and haze formation over an Eastern Asia megacity, Shanghai,

468 Atmospheric Environment, 92, 76-86, 10.1016/j.atmosenv.2014.04.007, 2014.

469 Massling, A., Stock, M., Wehner, B., Wu, Z. J., Hu, M., Bruggemann, E., Gnauk, T., Herrmann, H., and
470 Wiedensohler, A.: Size segregated water uptake of the urban submicrometer aerosol in Beijing,
471 Atmospheric Environment, 43, 1578-1589, 2009.

472 Momenimovahed, A., and Olfert, J. S.: Effective density and volatility of particles emitted from gasoline
473 direct injection vehicles and implications for particle mass measurement, Aerosol Sci. Technol., 49, 1051-
474 1062, 10.1080/02786826.2015.1094181, 2015.

475 Niu, H. Y., Hu, W., Zhang, D. Z., Wu, Z. J., Guo, S., Pian, W., Cheng, W. J., and Hu, M.: Variations of
476 fine particle physiochemical properties during a heavy haze episode in the winter of Beijing, Science of
477 the Total Environment, 571, 103-109, 10.1016/j.scitotenv.2016.07.147, 2016.

478 Olfert, J. S., Symonds, J. P. R., and Collings, N.: The effective density and fractal dimension of particles
479 emitted from a light-duty diesel vehicle with a diesel oxidation catalyst, Journal of Aerosol Science, 38,
480 69-82, 10.1016/j.jaerosci.2006.10.002, 2007.

481 Pagels, J., Khalizov, A. F., McMurry, P. H., and Zhang, R. Y.: Processing of Soot by Controlled Sulphuric
482 Acid and Water CondensationMass and Mobility Relationship, Aerosol Sci. Technol., 43, 629-640,
483 10.1080/02786820902810685, 2009.

484 Park, K., F., C., Kittelson, D. B., and McMurry, P. H.: Relationship between particle mass and mobility
485 for diesel exhaust particles Environmental Science and Technology, 37, 577-583, 2003.

Peng, J., Hu, M., Guo, S., Du, Z., Zheng, J., Shang, D., Zamora, M. L., Zeng, L., Shao, M., Wu, Y.-S., Zheng, J., Wang, Y., Glen, C. R., Collins, D. R., Molina, M. J., and Zhang, R.: Markedly enhanced absorption and direct radiative forcing of black carbon under polluted urban environments, Proceedings of the National Academy of Sciences of the United States of America, 113, 4266-4271, 10.1073/pnas.1602310113, 2016.

Petters, M. D., and Kreidenweis, S. M.: A single parameter representation of hygroscopic growth and cloud condensation nucleus activity, Atmospheric Chemistry and Physics, 7, 1961-1971, 2007.

Qiao, T., Zhao, M., Xiu, G., and Yu, J.: Simultaneous monitoring and compositions analysis of $PM_1$ and $PM_{2.5}$ in Shanghai: Implications for characterization of haze pollution and source apportionment, The Science of the total environment, 557-558, 386-394, 10.1016/j.scitotenv.2016.03.095, 2016.

Shi, Y., Chen, J., Hu, D., Wang, L., Yang, X., and Wang, X.: Airborne submicron particulate ($PM_1$) pollution in Shanghai, China: Chemical variability, formation/dissociation of associated semi-volatile components and the impacts on visibility, Science of the Total Environment, 473, 199-206, 10.1016/j.scitotenv.2013.12.024, 2014.

Spencer, M. T., Shields, L. G., and Prather, K. A.: Simultaneous measurement of the effective density and chemical composition of ambient aerosol particles, Environmental Science & Technology, 41, 1303-1309, 10.1021/es061425+, 2007.

Sun, Y. L., Chen, C., Zhang, Y. J., Xu, W. Q., Zhou, L. B., Cheng, X. L., Zheng, H. T., Ji, D. S., Li, J.,



504 Tang, X., Fu, P. Q., and Wang, Z. F.: Rapid formation and evolution of an extreme haze episode in
505 Northern China during winter 2015, Scientific Reports, 6, 10.1038/srep27151, 2016.
506 Swietlicki, E., Hansson, H. C., Hameri, K., Svenningsson, B., Massling, A., McFiggans, G., McMurry, P.
507 H., Petaja, T., Tunved, P., Gysel, M., Topping, D., Weingartner, E., Baltensperger, U., Rissler, J.,
508 Wiedensohler, A., and Kulmala, M.: Hygroscopic properties of submicrometer atmospheric aerosol
509 particles measured with H-TDMA instruments in various environments - a review, Tellus Ser. B-Chem.
510 Phys. Meteorol., 60, 432-469, 10.1111/j.1600-0889.2008.00350.x, 2008.
511 Tao, Y., Ye, X. N., Ma, Z., Xie, Y. Y., Wang, R. Y., Chen, J. M., Yang, X., and Jiang, S. Q.: Insights into
512 different nitrate formation mechanisms from seasonal variations of secondary inorganic aerosols in
513 Shanghai, Atmospheric Environment, 145, 1-9, 10.1016/j.atmosenv.2016.09.012, 2016.
514 Topping, D. O., McFiggans, G. B., and Coe, H.: A curved multi-component aerosol hygroscopicity model
515 framework: Part 1 - Inorganic compounds, Atmospheric Chemistry and Physics, 5, 1205-1222, 2005.
516 Wang, G., Zhang, R., Gomez, M. E., Yang, L., Zamora, M. L., Hu, M., Lin, Y., Peng, J., Guo, S., Meng,
517 J., Li, J., Cheng, C., Hu, T., Ren, Y., Wang, Y., Gao, J., Cao, J., An, Z., Zhou, W., Li, G., Wang, J., Tian,
518 P., Marrero-Ortiz, W., Secrest, J., Du, Z., Zheng, J., Shang, D., Zeng, L., Shao, M., Wang, W., Huang, Y.,
519 Wang, Y., Zhu, Y., Li, Y., Hu, J., Pan, B., Cai, L., Cheng, Y., Ji, Y., Zhang, F., Rosenfeld, D., Liss, P. S.,
520 Duce, R. A., Kolb, C. E., and Molina, M. J.: Persistent sulfate formation from London Fog to Chinese
521 haze, Proceedings of the National Academy of Sciences of the United States of America, 113, 13630-



522 13635, 10.1073/pnas.1616540113, 2016.

523 Wang, H., Xu, J., Zhang, M., Yang, Y., Shen, X., Wang, Y., Chen, D., and Guo, J.: A study of the
524 meteorological causes of a prolonged and severe haze episode in January 2013 over central-eastern China,
525 Atmospheric Environment, 98, 146-157, 10.1016/j.atmosenv.2014.08.053, 2014a.

526 Wang, Y., Wan, Q., Meng, W., Liao, F., Tan, H., and Zhang, R.: Long-term impacts of aerosols on
527 precipitation and lightning over the Pearl River Delta megacity area in China, Atmospheric Chemistry
528 and Physics, 11, 12421-12436, 10.5194/acp-11-12421-2011, 2011.

529 Wang, Y., Khalizov, A., Levy, M., and Zhang, R.: New Directions: Light absorbing aerosols and their
530 atmospheric impacts, Atmospheric Environment, 81, 713-715, 10.1016/j.atmosenv.2013.09.034, 2013.

531 Wang, Y., Zhang, Q., Jiang, J., Zhou, W., Wang, B., He, K., Duan, F., Zhang, Q., Philip, S., and Xie, Y.:
532 Enhanced sulfate formation during China's severe winter haze episode in January 2013 missing from
533 current models, J. Geophys. Res.-Atmos., 119, 10.1002/2013jd021426, 2014b.

534 Wang, Y., Zhang, R., and Saravanan, R.: Asian pollution climatically modulates mid-latitude cyclones
535 following hierarchical modelling and observational analysis, Nature Communications, 5,
536 10.1038/ncomms4098, 2014c.

537 Wang, Y. H., Liu, Z. R., Zhang, J. K., Hu, B., Ji, D. S., Yu, Y. C., and Wang, Y. S.: Aerosol
538 physicochemical properties and implications for visibility during an intense haze episode during winter
539 in Beijing, Atmospheric Chemistry and Physics, 15, 3205-3215, 10.5194/acp-15-3205-2015, 2015.

Wu, G., Li, Z., Fu, C., Zhang, X., Zhang, R., Zhang, R., Zhou, T., Li, J., Li, J., Zhou, D., Wu, L., Zhou, L., He, B., and Huang, R.: Advances in studying interactions between aerosols and monsoon in China, Science China-Earth Sciences, 59, 1-16, 10.1007/s11430-015-5198-z, 2016a.

Wu, S., Ni, Y., Li, H., Pan, L., Yang, D., Baccarelli, A. A., Deng, F., Chen, Y., Shima, M., and Guo, X.: Short-term exposure to high ambient air pollution increases airway inflammation and respiratory symptoms in chronic obstructive pulmonary disease patients in Beijing, China, Environment International, 94, 76-82, 10.1016/j.envint.2016.05.004, 2016b.

Xiao, S., Wang, Q. Y., Cao, J. J., Huang, R. J., Chen, W. D., Han, Y. M., Xu, H. M., Liu, S. X., Zhou, Y. Q., Wang, P., Zhang, J. Q., and Zhan, C. L.: Long-term trends in visibility and impacts of aerosol composition on visibility impairment in Baoji, China, Atmospheric Research, 149, 88-95, 10.1016/j.atmosres.2014.06.006, 2014.

Xiao, S., Wang, M. Y., Yao, L., Kulmala, M., Zhou, B., Yang, X., Chen, J. M., Wang, D. F., Fu, Q. Y., Worsnop, D. R., and Wang, L.: Strong atmospheric new particle formation in winter in urban Shanghai, China, Atmospheric Chemistry and Physics, 15, 1769-1781, 10.5194/acp-15-1769-2015, 2015.

Xie, Y., Ding, A., Nie, W., Mao, H., Qi, X., Huang, X., Xu, Z., Kerminen, V.-M., Petaja, T., Chi, X., Virkkula, A., Boy, M., Xue, L., Guo, J., Sun, J., Yang, X., Kulmala, M., and Fu, C.: Enhanced sulfate formation by nitrogen dioxide: Implications from in situ observations at the SORPES station, J. Geophys. Res.-Atmos., 120, 12679-12694, 10.1002/2015jd023607, 2015.

558 Yang, L., Zhou, X., Wang, Z., Zhou, Y., Cheng, S., Xu, P., Gao, X., Nie, W., Wang, X., and Wang, W.:
559 Airborne fine particulate pollution in Jinan, China: Concentrations, chemical compositions and influence
560 on visibility impairment, Atmospheric Environment, 55, 506-514, 10.1016/j.atmosenv.2012.02.029, 2012.
561 Ye, X. N., Chen, T. Y., Hu, D. W., Yang, X., Chen, J. M., Zhang, R. Y., Khakuziv, A. F., and Wang, L.: A
562 multifunctional HTDMA system with a robust temperature control, Advances in Atmospheric Sciences,
563 26, 1235-1240, 10.1007/s00376-009-8134-3, 2009.
564 Ye, X. N., Ma, Z., Hu, D. W., Yang, X., and Chen, J. M.: Size-resolved hygroscopicity of submicrometer
565 urban aerosols in Shanghai during wintertime, Atmospheric Research, 99, 353-364, 2010.
566 Ye, X. N., Ma, Z., Zhang, J. C., Du, H. H., Chen, J. M., Chen, H., Yang, X., Gao, W., and Geng, F. H.:
567 Important role of ammonia on haze formation in Shanghai, Environ Res Lett, 6, Artn 024019
568 Doi 10.1088/1748-9326/6/2/024019, 2011.
569 Ye, X. N., Tang, C., Yin, Z., Chen, J. M., Ma, Z., Kong, L. D., Yang, X., Gao, W., and Geng, F. H.:
570 Hygroscopic growth of urban aerosol particles during the 2009 Mirage-Shanghai Campaign, Atmospheric
571 Environment, 64, 263-269, 10.1016/j.atmosenv.2012.09.064, 2013.
572 Yin, Z., Ye, X., Jiang, S., Tao, Y., Shi, Y., Yang, X., and Chen, J.: Size-resolved effective density of urban
573 aerosols in Shanghai, Atmospheric Environment, 100, 133-140, 10.1016/j.atmosenv.2014.10.055, 2015.
574 Zhang, Q., Quan, J., Tie, X., Li, X., Liu, Q., Gao, Y., and Zhao, D.: Effects of meteorology and secondary
575 particle formation on visibility during heavy haze events in Beijing, China, Science of The Total

576 Environment, 502, 578-584, http://dx.doi.org/10.1016/j.scitotenv.2014.09.079, 2015a.

577 Zhang, R., Khalizov, A., Wang, L., Hu, M., and Xu, W.: Nucleation and Growth of Nanoparticles in the
578 Atmosphere, Chemical Reviews, 112, 1957-2011, 10.1021/cr2001756, 2012.

579 Zhang, R., Guo, S., Zamora, M. L., and Hu, M.: Reply to Li et al.: Insufficient evidence for the
580 contribution of regional transport to severe haze formation in Beijing, Proceedings of the National
581 Academy of Sciences of the United States of America, 112, E2741-E2741, 10.1073/pnas.1503855112,
582 2015b.

583 Zhang, R., Wang, G., Guo, S., Zarnora, M. L., Ying, Q., Lin, Y., Wang, W., Hu, M., and Wang, Y.:
584 Formation of Urban Fine Particulate Matter, Chemical Reviews, 115, 3803-3855,
585 10.1021/acs.chemrev.5b00067, 2015c.

586 Zhang, R. Y., Suh, I., Zhao, J., Zhang, D., Fortner, E. C., Tie, X. X., Molina, L. T., and Molina, M. J.:
587 Atmospheric new particle formation enhanced by organic acids, Science, 304, 1487-1490,
588 10.1126/science.1095139, 2004.

589 Zhang, R. Y., Khalizov, A. F., Pagels, J., Zhang, D., Xue, H. X., and McMurry, P. H.: Variability in
590 morphology, hygroscopicity, and optical properties of soot aerosols during atmospheric processing,
591 Proceedings of the National Academy of Sciences of the United States of America, 105, 10291-10296,
592 2008.

593 Zhao, J., Khalizov, A., Zhang, R., and McGraw, R.: Hydrogen-Bonding Interaction in Molecular

Complexes and Clusters of Aerosol Nucleation Precursors, Journal of Physical Chemistry A, 113, 680-689, 10.1021/jp806693r, 2009.

Zhao, X. J., Zhao, P. S., Xu, J., Meng, W., Pu, W. W., Dong, F., He, D., and Shi, Q. F.: Analysis of a winter regional haze event and its formation mechanism in the North China Plain, Atmospheric Chemistry and Physics, 13, 5685-5696, 10.5194/acp-13-5685-2013, 2013.

Zheng, G. J., Duan, F. K., Su, H., Ma, Y. L., Cheng, Y., Zheng, B., Zhang, Q., Huang, T., Kimoto, T., Chang, D., Poeschl, U., Cheng, Y. F., and He, K. B.: Exploring the severe winter haze in Beijing: the impact of synoptic weather, regional transport and heterogeneous reactions, Atmospheric Chemistry and Physics, 15, 2969-2983, 10.5194/acp-15-2969-2015, 2015.

Atmos. Chem. Phys. Discuss., doi:10.5194/acp-2017-16, 2017
Manuscript under review for journal Atmos. Chem. Phys.
Discussion started: 16 February 2017


Atmospheric Chemistry and Physics Discussions

## Figure and Table Captions

Figure 1 Schematic diagram of HTDMA-APM system.

Figure 2. Temporal evolutions of $PM_{1.0}$, $PM_{2.5}$, and $PM_{10}$ concentrations during the winter observation.

Figure 3 Variations of sulfate, nitrate, and ammonium concentrations as a function of $PM_{1.0}$ mass loading.

Figure 4 Box plots showing hygroscopicity parameter and effective density at each dry diameter over the whole observation. The whiskers represent the $5^{th}$ and $95^{th}$ percentile, the two borders of box display the $25^{th}$ and $75^{th}$ percentile, and the band in each box denotes the median.

Figure 5 Temporal evolutions of particle number size distribution (A), volume size distribution (B), total number concentration and total volume concentration (C), and $PM_{1.0}$ concentration and calculated PM (less than 600 nm in mobility diameter) concentration during the representative PM episode from 7 to 12 January.

Figure 6 Evolutions of particle hygroscopic growth factor and effective density for different sizes during the representative PM episode.

Figure 7 Temporal evolutions of chemical compositions determined by SPAMS during the representative PM episode.

Figure 8 Particle hygroscopicity and density during the two particle growth processes

Atmos. Chem. Phys. Discuss., doi:10.5194/acp-2017-16, 2017
Manuscript under review for journal Atmos. Chem. Phys.
Discussion started: 16 February 2017


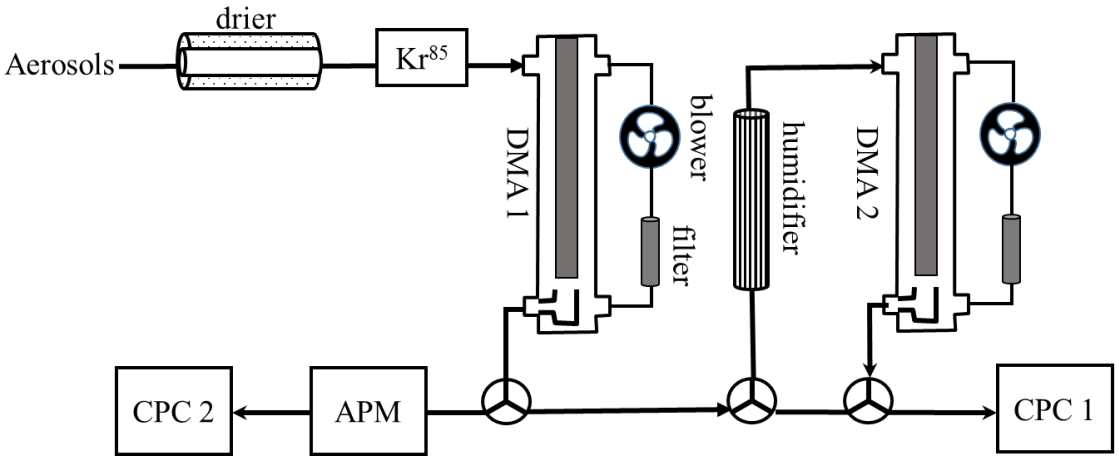


Figure 1 Schematic diagram of HTDMA-APM system.

Atmos. Chem. Phys. Discuss., doi:10.5194/acp-2017-16, 2017
Manuscript under review for journal Atmos. Chem. Phys.
Discussion started: 16 February 2017


Atmospheric Chemistry and Physics Discussions

629

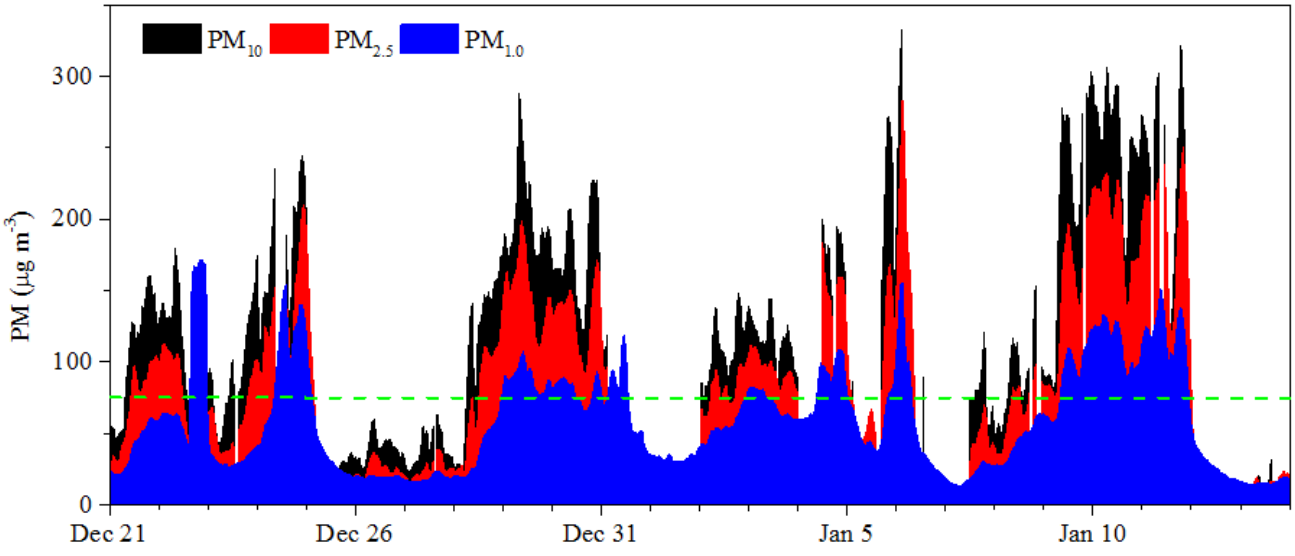


630

631 Figure 2. Temporal evolutions of $PM_{1.0}$, $PM_{2.5}$, and $PM_{10}$ concentrations during the winter observation.

632

Atmos. Chem. Phys. Discuss., doi:10.5194/acp-2017-16, 2017
Manuscript under review for journal Atmos. Chem. Phys.
Discussion started: 16 February 2017


Atmospheric Chemistry and Physics Discussions

633

634

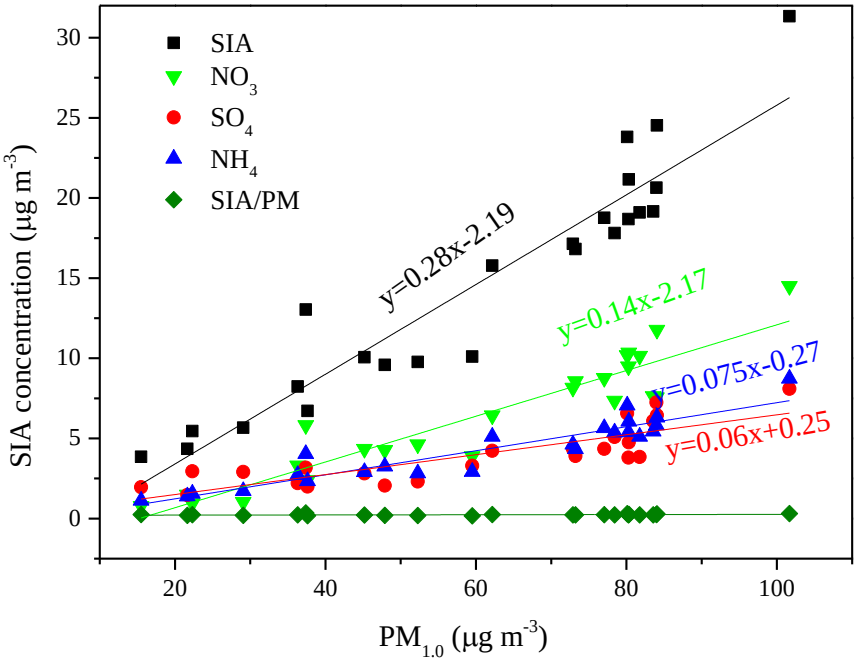


635

636 Figure 3 Variations of sulfate, nitrate, and ammonium concentrations as a function of $PM_{1.0}$ mass loading

637

Atmos. Chem. Phys. Discuss., doi:10.5194/acp-2017-16, 2017
Manuscript under review for journal Atmos. Chem. Phys.
Discussion started: 16 February 2017


Atmospheric Chemistry and Physics Discussions

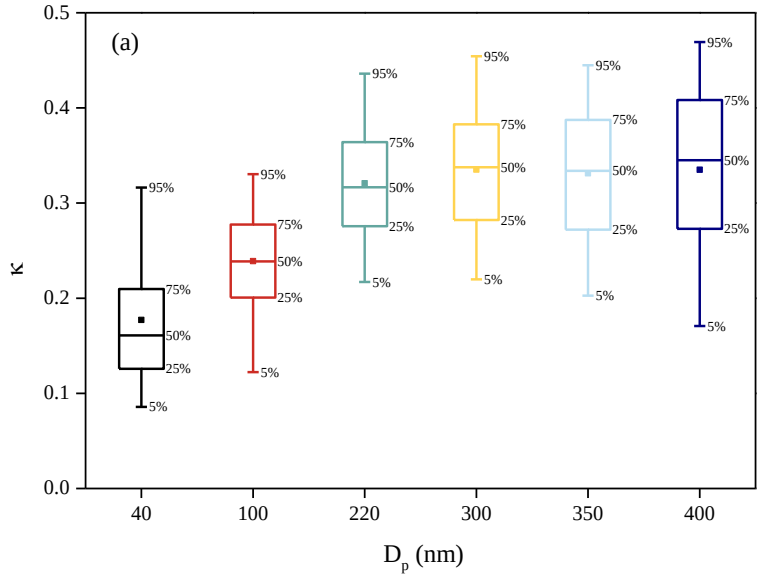


638

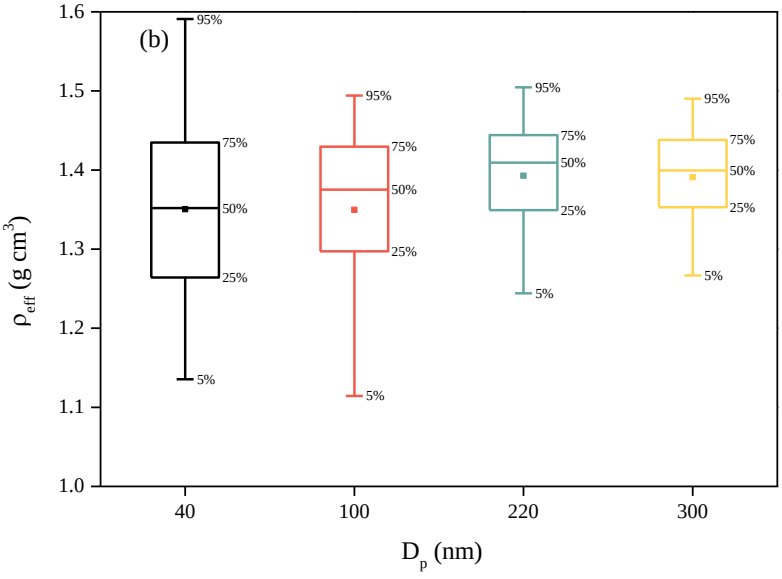


639

640 Figure 4 Box plots showing hygroscopicity parameter and effective density at each dry diameter over the
641 whole observation. The whiskers represent the 5$^{th}$ and 95$^{th}$ percentile, the two borders of box display the
642 25$^{th}$ and 75$^{th}$ percentile, and the band in each box denotes the median.

Atmos. Chem. Phys. Discuss., doi:10.5194/acp-2017-16, 2017
Manuscript under review for journal Atmos. Chem. Phys.
Discussion started: 16 February 2017


643

644

645

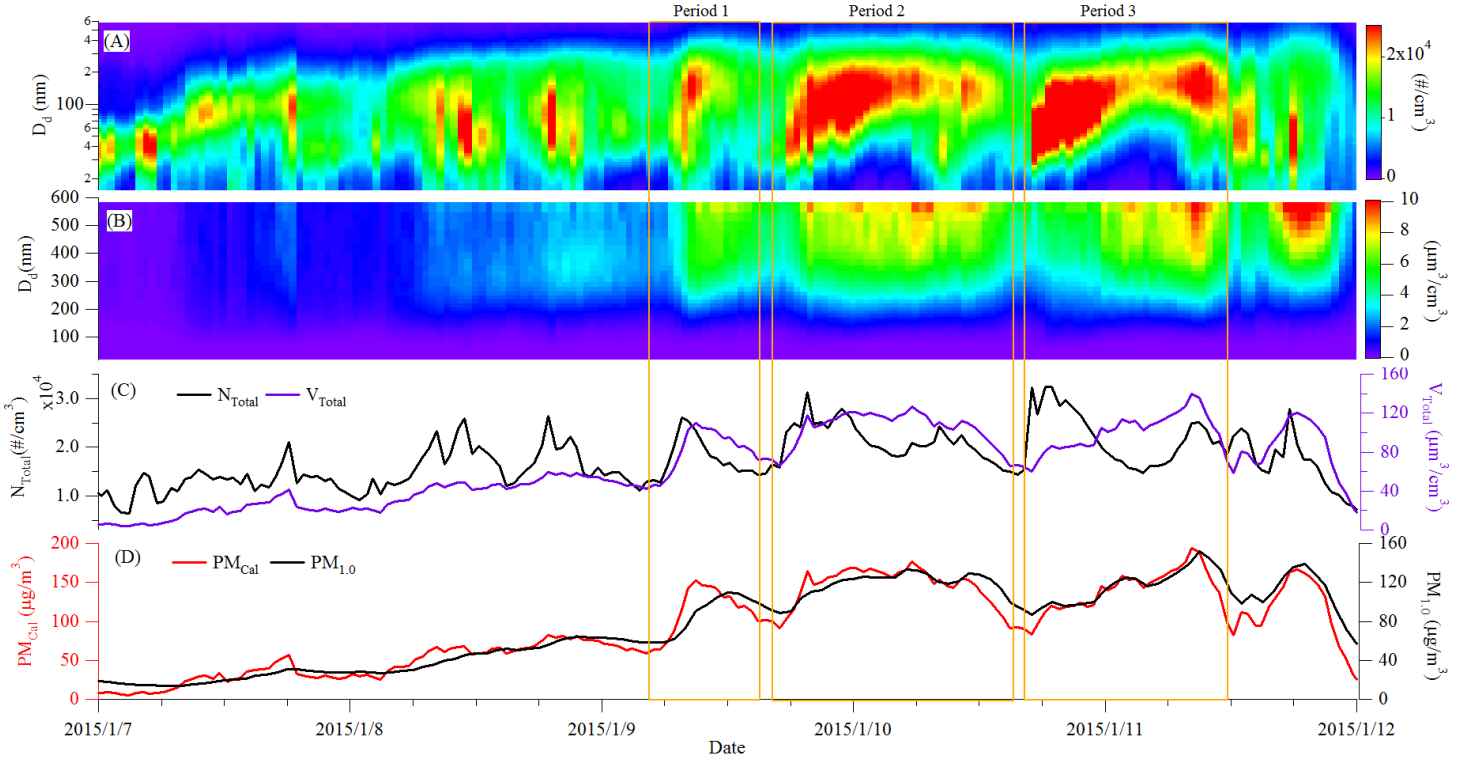


646

647 Figure 5 Temporal evolutions of particle number size distribution (A), volume size distribution (B), total
648 number concentration and total volume concentration (C), and $PM_{1.0}$ concentration and calculated PM
649 (less than 600 nm in mobility diameter) concentration during the representative PM episode from 7 to 12
650 January.

651

652

653

Atmos. Chem. Phys. Discuss., doi:10.5194/acp-2017-16, 2017
Manuscript under review for journal Atmos. Chem. Phys.
Discussion started: 16 February 2017


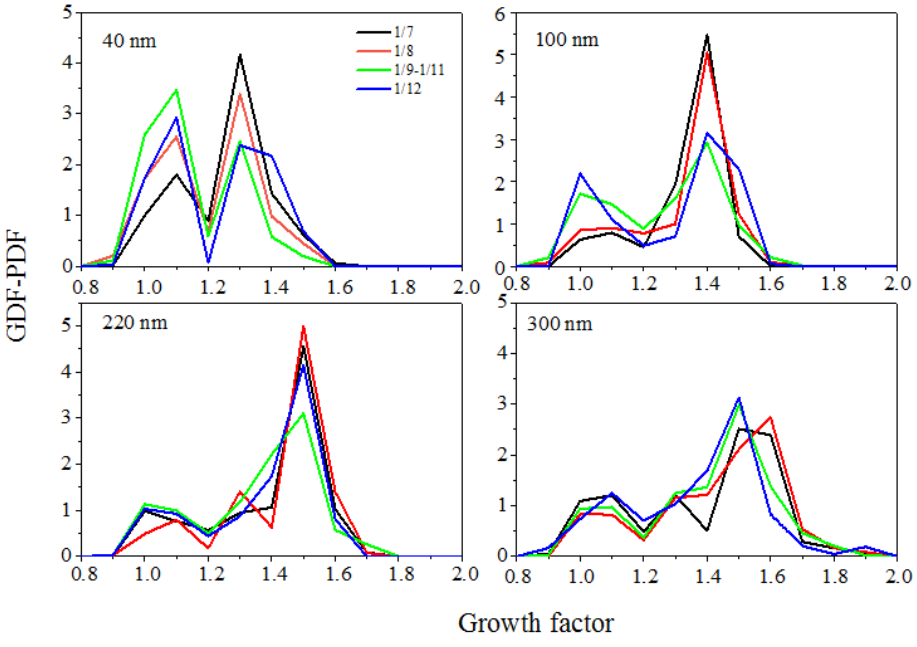


654

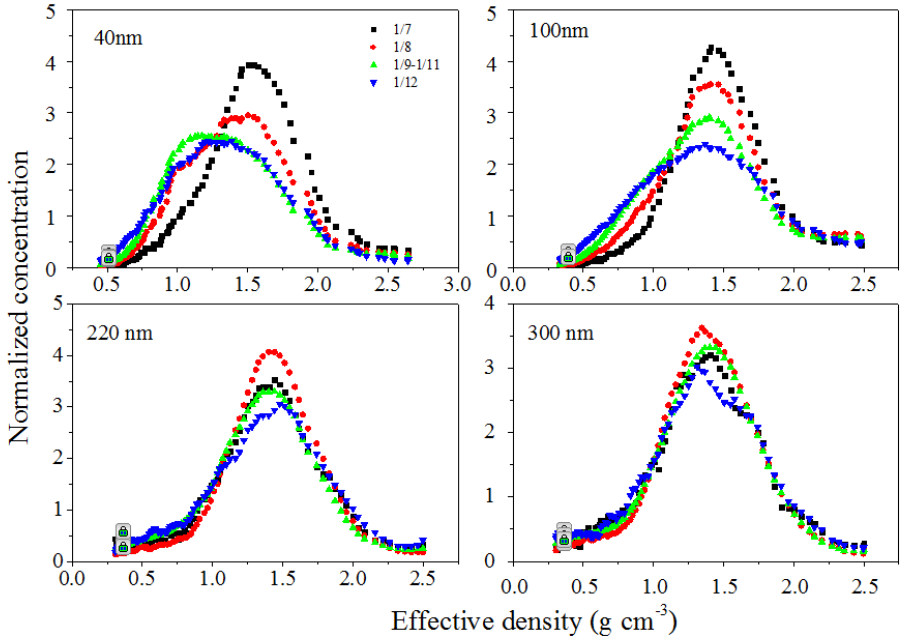


655

656 Figure 6 Evolutions of particle hygroscopic growth factor and effective density for different sizes during
657 the representative PM episode.

Atmos. Chem. Phys. Discuss., doi:10.5194/acp-2017-16, 2017
Manuscript under review for journal Atmos. Chem. Phys.
Discussion started: 16 February 2017


Atmospheric Chemistry and Physics Discussions

658
659
660

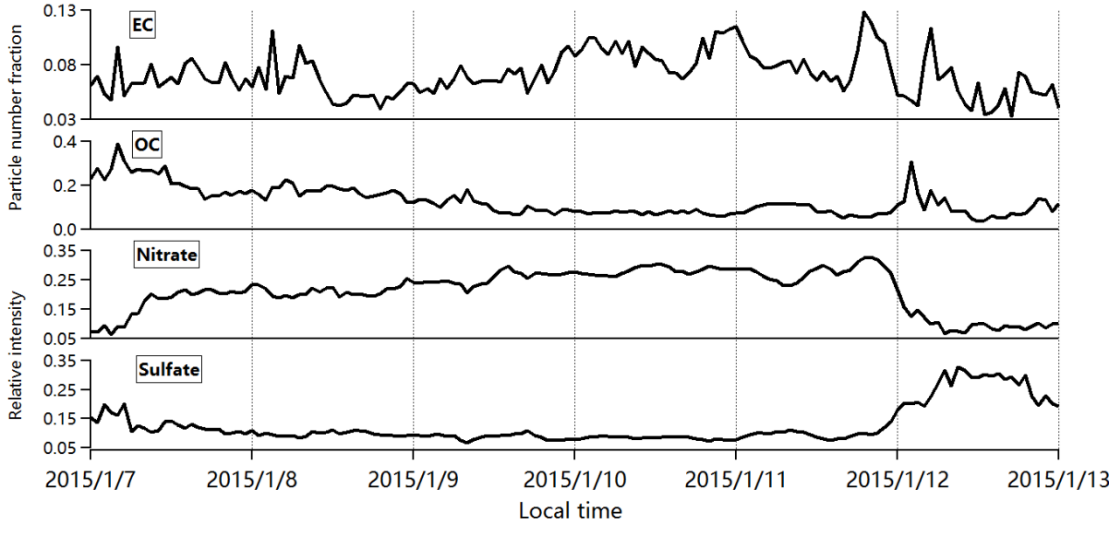


661

662 Figure 7 Temporal evolutions of chemical compositions determined by SPAMS during the representative
663 PM episode.

664

Atmos. Chem. Phys. Discuss., doi:10.5194/acp-2017-16, 2017
Manuscript under review for journal Atmos. Chem. Phys.
Discussion started: 16 February 2017


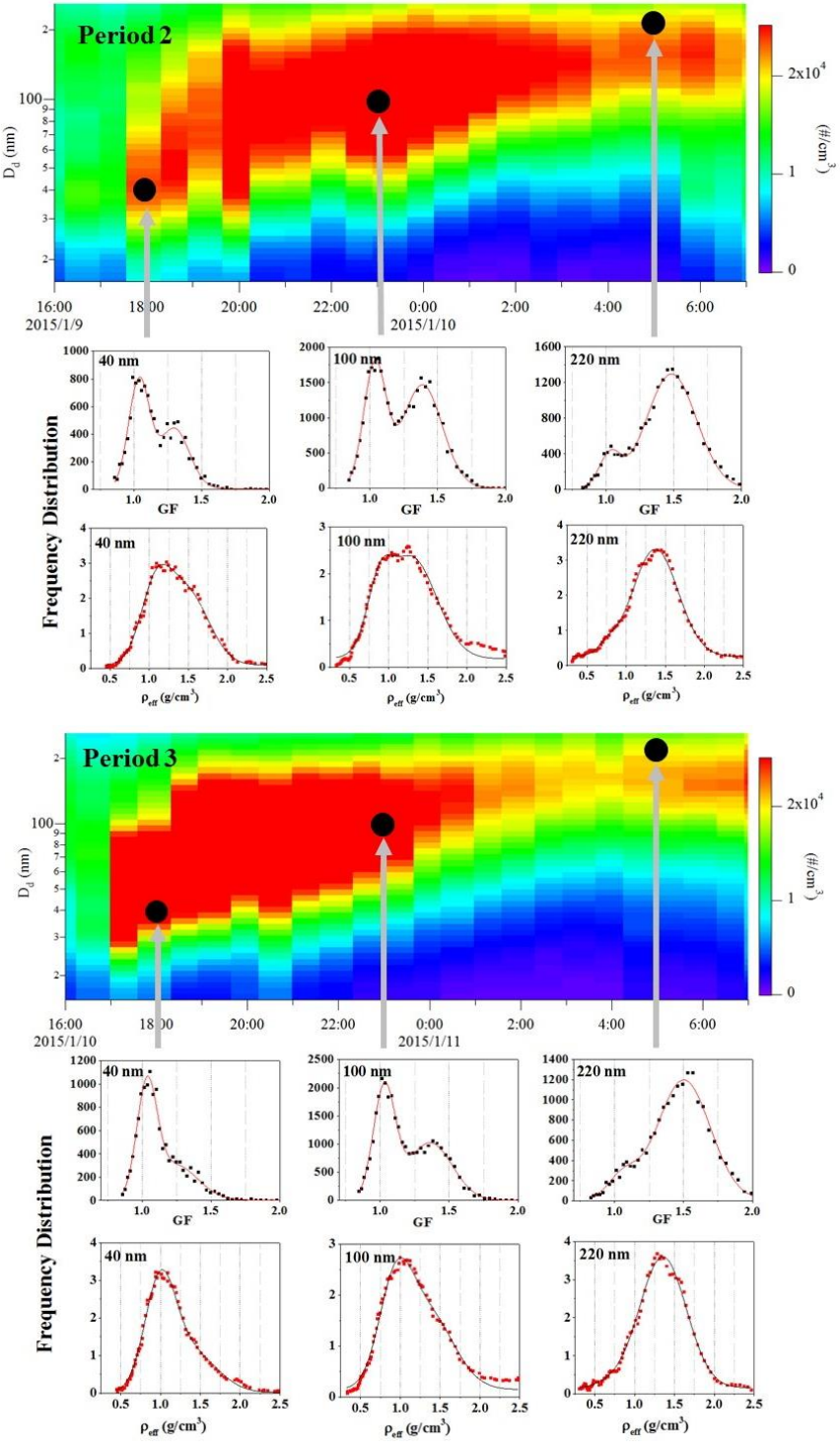


Figure 8 Particle hygroscopicity and density during the two particle growth processes.